

Brief investigations on $Cu_xTa_{2-x}O_5$ for thermoelectric and optical responses using density functional and experimental techniques

Laiba Ashraf, Salma Waseem, Maria Khalil, Naveed Ahmad, Pervaiz Ahmad, Imen Kebaili, and Murtaza Saleem

Citation: Chin. Phys. B, 2026, 35 (**2**): 027801. DOI: 10.1088/1674-1056/adee89
http://cpb.iphy.ac.cn; http://iopscience.iop.org/cpb

What follows is a list of articles you may be interested in

Optical study of magnetic topological insulator $MnBi_4Te_7$

Zhi-Yu Liao(廖知裕), Bing Shen(沈冰), Xiang-Gang Qiu(邱祥冈), and Bing Xu(许兵)
Chin. Phys. B, 2024, 33 (**1**): 017802. DOI: 10.1088/1674-1056/ad08aa

Unveiling localized electronic properties of ReS_2 thin layers at nanoscale using Kelvin force probe microscopy combined with tip-enhanced Raman spectroscopy

Yu Luo(罗宇), Weitao Su(苏伟涛), Juanjuan Zhang(张娟娟), Fei Chen(陈飞), Ke Wu(武可), Yijie Zeng(曾宜杰), and Hongwei Lu(卢红伟)
Chin. Phys. B, 2023, 32 (**11**): 117801. DOI: 10.1088/1674-1056/ace425

Theoretical investigation on the fluorescent sensing mechanism for recognizing formaldehyde: TDDFT calculation and excited-state nonadiabatic dynamics

Yunfan Yang(杨云帆), Lujia Yang(杨璐佳), Fengcai Ma(马凤才), Yongqing Li(李永庆), and Yue Qiu(邱岳)
Chin. Phys. B, 2023, 32 (**5**): 057801. DOI: 10.1088/1674-1056/ac80af

Achieving high-performance multilayer $MoSe_2$ photodetectors by defect engineering

Jintao Hong(洪锦涛), Fengyuan Zhang(张丰源), Zheng Liu(刘峥), Jie Jiang(蒋杰), Zhangting Wu(吴章婷), Peng Zheng(郑鹏), Hui Zheng(郑辉), Liang Zheng(郑梁), Dexuan Huo(霍德璇), Zhenhua Ni(倪振华), and Yang Zhang(张阳)
Chin. Phys. B, 2021, 30 (**8**): 087801. DOI: 10.1088/1674-1056/abea8b

A theoretical study on chemical ordering of 38-atom trimetallic Pd-Ag-Pt nanoalloys

Songül Taran, Ali Kemal Garip, Haydar Arslan
Chin. Phys. B, 2020, 29 (**7**): 077801. DOI: 10.1088/1674-1056/ab99b4

Brief investigations on $Cu_xTa_{2-x}O_5$ for thermoelectric and optical responses using density functional and experimental techniques

Laiba Ashraf[1], Salma Waseem[1], Maria Khalil[2,3], Naveed Ahmad[4], Pervaiz Ahmad[5], Imen Kebaili[6], and Murtaza Saleem[7,†]

[1] *Department of Physics, Lahore College for Women University, Lahore* 54600, *Pakistan*
[2] *Department of Physics, University of the Punjab, Quaid-e-Azam Campus, Lahore* 54000, *Pakistan*
[3] *Department of Physics, Mirpur University of Science and Technology (MUST), AJK, Mirpur,* 10250, *Pakistan*
[4] *Department of Chemical and Materials Engineering, College of Engineering, Northern Border University, Arar, Saudi Arabia*
[5] *Department of Physics, College of Science and Humanities, Prince Sattam Bin Abdulaziz University, P. O. Box* 173, *Al-Kharj* 11942, *Saudi Arabia*
[6] *Departmentt of Physics, Faculty of Science, King Khalid University, P. O. Box* 960, *Abha, Saudi Arabia*
[7] *Department of Physics, SBASSE, Lahore University of Management Sciences, Lahore* 54792, *Pakistan*

(Received 2 April 2025; revised manuscript received 4 July 2025; accepted manuscript online 11 July 2025)

$Cu_xTa_{2-x}O_5$ compositions were investigated for advanced thermoelectric and optical applications, using both simulations and experimental approaches. Density functional theory calculations were performed before the experimental observations to predict the trends of various parameters. Crystal structure analysis confirmed the presence of the orthorhombic Ta_2O_5 phase in all the compositions. The composition and morphology demonstrated impurity-free contents with uniform and crack-free surfaces. Thermoelectric analysis depicted a decrease in Seebeck coefficient from 3.66 $\mu V \cdot K^{-1}$ to 1.91 $\mu V \cdot K^{-1}$ and an increase in the value of specific heat from 0.73 $J \cdot K^{-1} \cdot kg^{-1}$ to 11.6 $J \cdot K^{-1} \cdot kg^{-1}$ upon Cu incorporation in structure. The bandgap was found to reduce from 2.61 to 1.38 eV with Cu-induced electronic states. The real epsilon and static refractive index increased from 3.75 to 4.57 and from 1.93 to 2.11, respectively, with increment in Cu content. The enhanced parameters, focusing on the thermoelectric and optical responses, make these compositions potential candidates for advanced optoelectronic applications.

Keywords: Ta_2O_5, DFT, electronic properties, thermoelectric properties, optical properties

PACS: 78.20.–e, 77.84.Bw, 71.15.Mb, 73.50.Lw, 73.61.–r

DOI: 10.1088/1674-1056/adee89 **CSTR:** 32038.14.CPB.adee89

1. Introduction

In recent years, researchers have focused on transition metal oxides owing to their unique optical, electrical, magnetic, thermoelectric, and electrochemical properties.[1] Among different transition metal oxides, tantalum oxide (Ta_2O_5) is a potential semiconductor with distinctive features, including a large bandgap of 3.9 eV, high resistivity, high ε of approximately 50–70, good breakdown field strength, high-temperature piezoelectric properties, low leakage current, chemical stability, high ionic conductivity, low internal stress, high biocompatibility, good thermal and mechanical stabilities, and high refractive index of 2.125.[2–10] In addition to its many properties, Ta_2O_5 has intriguing structural characteristics. It is amorphous at temperatures below 650 °C. Nevertheless, when crystalline, it can take on a variety of shapes, including those that are oxygen-rich and oxygen-deficient. It is evident that at approximately 1360 °C, the low-temperature (L) crystalline phase gives rise to a high-temperature (H) crystalline phase.[11–13]

The incorporation of dopants into Ta_2O_5 significantly influences its structural, electrical, and optical properties, which enhances its functionality in various technological applications. Doping influences electrical conductivity by creating defect states or charge carriers. For example, tungsten doping enhances conductivity by acting as a donor state, thereby establishing Ta_2O_5 as an active layer material for UV detectors.[14] Nitrogen doping in Ta_2O_5 lowers the bandgap and enhances the visible light absorption for photocatalysis. It further improves charge separation by creating oxygen vacancies and increases the efficiency of water splitting.[15] Ta_2O_5 is chemically significant because of its complex crystal structure, which permits the incorporation of a variety of dopant ions at high concentrations with minimal structural changes.[16] However, copper (Cu) is a valuable dopant because of its superior electronic conductivity and affordability. According to previous reports, Cu-doped TiO_2 and CuO/TiO_2 composites are effective photocatalytic materials for the degradation of dyes, organic pollutants, and other substances. Cu doping in metal oxides creates defects and d-band states that reduce the bandgap of the semiconductor oxides. It acts as an electron trap, which lowers carrier recombination and enhances charge separation.[17,18] ZnS-Cu and ZnO-Cu are light-emitting materials, in which cop-

†Corresponding author. E-mail: murtaza.saleem@lums.edu.pk

© 2026 Chinese Physical Society and IOP Publishing Ltd. All rights, including for text and data mining, AI training, and similar technologies, are reserved.

per serves as a transition metal dopant, tuning the electronic structure and improving optical efficiency.[19] Thus, there are several methods for depositing Ta_2O_5 films, including electron beam evaporation,[20] chemical vapor deposition,[21] sputtering,[22,23] sol–gel synthesis,[24] and pulse laser deposition (PLD).[25] Co-sputtering was selected because of its target purity, ease of doping control, and ability to attain high dopant concentrations.[26]

Previous studies have shown that $Cu_xTa_{2-x}O_5$ compositions remain unexplored in terms of their thermoelectric and optical responses. In this brief study, density functional theory (DFT) calculations were used to predict the trends of various parameters. Similar compositions were experimentally fabricated in uniform and phase-pure structures using magnetron sputtering for comparative analysis. DFT-based calculations provide insights into the electronic band structure and thermoelectric and optical properties. The trends of various parameters predicted through simulations were experimentally observed to check the suitability of these compositions for advanced applications.

2. Computational and experimental methods

2.1. Computational method

Density functional theory (DFT) calculations were performed using the FP-LAPW method in WIEN2k to investigate the optical, electrical, and thermoelectric properties of pure and Cu-doped Ta_2O_5. To represent different Cu doping levels in Ta_2O_5, different supercell sizes were used by replacing one Ta atom with Cu: a $4\times2\times2$ supercell for 4.16%, a $2\times2\times2$ supercell for 6.25%, and a $1\times2\times2$ supercell for 12.5%. A Hubbard U value of 4.0 eV was chosen for Ta 5d orbitals based on previous reports, where similar values successfully represented the electronic structure of Ta_2O_5. To assess the effect of the U parameter, additional calculations were performed within the 3.0–5.0 eV range. The resulting shifts in the band edges were minimal, and the main features of the TDOS and PDO, including the changes attributable to Cu incorporation, remained stable. This confirmed the reliability of the selected U value for describing the electronic properties of the system. The TB-mBJ functional was used for an accurate bandgap estimation. The computational parameters included a plane wave cutoff energy of -6 Ry, $RK_{\max}$ of 7.0, $G_{\max}$ of 12, and $l_{\max}$ of 10. A 1000 k-point grid ensured a precise Brillouin zone integration. The SCF calculations were converged with an energy threshold of 10^{-3} eV and a charge convergence of 10^{-4} C. The thermoelectric properties were assessed via BoltzTraP under constant relaxation time approximation.

2.2. Experimental method

Experimental deposition of the simulated compositions of pure and Cu-doped Ta_2O_5 on silicon-100 substrates was conducted using a DC magnetron co-sputtering (DAON 1000S) system under O_2/Ar ambient conditions at room temperature. Pure Ta_2O_5 thin films were deposited by loading a tantalum metallic target and an oxygen-reactive gas into a DC sputtering gun. Cu-doped Ta_2O_5 thin films were synthesized by co-sputtering Cu and Ta targets into two separate sputtering guns controlled by a DC power source. Through a power supply adjustment, the DC power supply connected to the sputter gun controlled the composition of the material. Using a turbo pumping station, an initial vacuum of 1×10^{-6} Torr was maintained before each thin film deposition. The flow rates of argon and oxygen gas were adjusted to 70 sccm and 30 sccm, respectively, and the working pressure of 5 mTorr was maintained during the deposition process. The chamber's Sycon thickness monitor was used to regulate the sputtering speeds for the Cu-Ta_2O_5 thin films to achieve the desired composition and thickness. Finally, in the muffle furnace, the thin films that were formed were thermally annealed for 4 h at 800 °C. The pure and Cu-doped Ta_2O_5 thin films were analyzed using various characterization techniques.

The phase and crystallographic patterns of the thin films that formed were examined using a Bruker D2-phaser x-ray diffractometer (XRD) that used Cu-$K\alpha$ radiation. An FEI Nova NanoSEM 450 field emission scanning electron microscopy (FESEM) and Oxford INCA x-act energy dispersive x-ray (EDX) spectroscopy were used to investigate the surface morphology and elemental compositions, respectively. The optical parameters were obtained using the Alpha-SE spectroscopic ellipsometry technique.

3. Results and discussion

3.1. X-ray diffraction analysis

Figures 1(a)–1(d) show the x-ray diffraction patterns of both pure and Cu-doped Ta_2O_5. The 2θ values ranged from 20° to 40°. All samples displayed almost identical diffraction patterns indexed by the (hkl) values of the characteristic peaks with variable diffracted line intensities and a slight positional change. There were two peaks in the composition with the respective Miller indices (110) and (019). The diffracted pattern of the thin films exhibited a Ta_2O_5 phase with an orthorhombic structure and dominant peaks that are well matched with JCPDS # 89–2843. No secondary phase was found in the XRD pattern, revealing the formation of single-phase Ta_2O_5. It was also observed that the addition of Cu decreased the peak intensity, indicating substitution of Cu in the Ta_2O_5 films, which might be caused by the incorporation of Cu, leading to a disturbance in the degree of crystallinity and distortion in the structure.

Structural factors play an important role in determining material behavior and qualities, particularly the microstructure, and how they are used in electronic devices.[27] In the

table, structural parameters such as FWHM, microstrain, crystallite size, and dislocation density are mentioned. Using Debye Scherrer's formula, the average crystallite size of the thin films was determined as $D = \frac{0.9\lambda}{\beta \cos\theta}$, where λ is the wavelength of the x-ray, β in full-width half-maxima, 0.9 is the value of the shape constant, and θ is the diffraction angle. The crystallite size of the most intense peak, which was located at 23.76 with *hkl* of (110), was calculated, as shown in Table 1. As Cu was added to the system, the intensity of the peaks decreased, indicating a decrease in FWHM, and as a result, the crystallite size increased. The dislocation density was calculated using $\delta = 1/D^2$, where D is the crystallite size, and the microstrain was calculated using $\varepsilon = \frac{\beta}{4\tan\theta}$. The results revealed the decrease in strain with the inclusion of Cu, and this reduction in strain enhanced the crystallite size. The dislocation density decreased as Ta_2O_5 was added to the system; therefore, the Cu-doped films had a more stable structure. Therefore, the results demonstrate the effect of Cu on the structural parameters, such as dislocation density, strain, and crystallite size. Structural analysis based on the XRD patterns revealed shifts in peak positions and variations in intensity, which indicate the inclusion of Cu atoms into the Ta_2O_5 lattice site and, consequently, slight lattice distortion. The observed decrease in microstrain and dislocation density, along with an increase in crystallite size, indicates that Cu doping enhances the crystal structure by minimizing the internal stresses and enhancing the crystal quality.

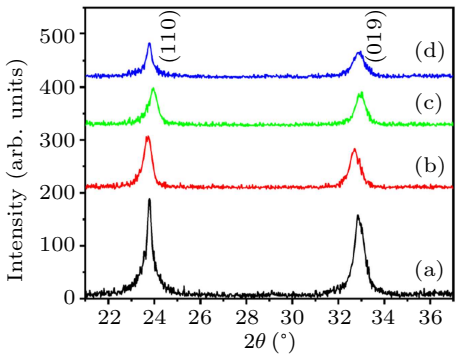


Fig. 1. XRD pattern of (a) Ta_2O_5, (b) 4.16% Cu-Ta_2O_5, (c) 6.25% Cu-Ta_2O_5, and (d) 12.5% Cu-Ta_2O_5 thin films.

Table 1. Structural parameters of Ta_2O_5 and Cu-doped Ta_2O_5 thin films.

Parameters	Ta_2O_5	4.16% Cu	6.25% Cu	12.5% Cu
2θ (°)	23.77	23.70	23.93	23.77
hkl	110	110	110	110
FWHM (°)	0.461	0.460	0.513	0.393
Crystallite size (nm)	17.59	17.61	15.81	20.61
Dislocation density (10^{-3} nm^{-2})	3.23	3.22	3.99	2.35
Microstrain (10^{-3})	9.55	9.57	10.56	8.15

3.2. FESEM and elemental composition analysis

The surface morphology analyzed using FESEM further confirmed the structural changes. Figure 2 shows the FESEM micrographs of the pure and Cu-doped Ta_2O_5 thin films. The images from the field emission scanning electron microscope were recorded using a lens detector with a 10 kV beam intensity in the secondary electron mode at 100k magnification while the distance between the pole pieces and sample was adjusted to 5.0 mm. The images indicate homogeneous thin films, leading to some agglomeration after doping, revealing the incorporation of Cu into the Ta_2O_5 films. All the samples in the figure exhibit compact structures without cracks, whereas micrometer-sized grains are uniformly distributed throughout the substrate. Figure 2(a) displays the surface morphology of a pure tantalum oxide thin film with a uniformly smooth surface that exhibits small, densely packed grains. Figure 2(b) illustrates that granule formation results from the addition of Cu with different sizes separated by sharp grain boundaries. With the increase in doping concentration, the variation in grain size and irregular shape can be observed in Figs. 2(c) and 2(d). Figure 2(c) depicts the formation of blisters with increasing Cu concentration owing to the agglomeration of smaller grains. Figure 2(d) demonstrates that with a further increase in Cu concentration, a significant reduction in grain boundaries was observed owing to the nucleation process, leading to roughness of the film surface. Therefore, the changes in morphology were attributable to changes in the Cu concentration, indicating that Cu acts as a nucleation center because it influences the nucleation process and growth of grains.

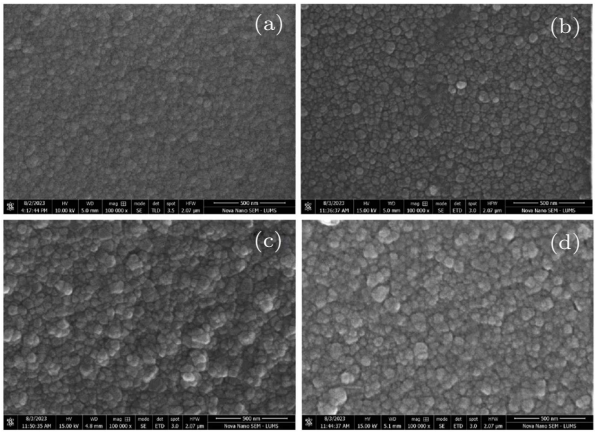


Fig. 2. FESEM micrographs of (a) pure Ta_2O_5, (b) 4.16% Cu-Ta_2O_5, (c) 6.25% Cu-Ta_2O_5, and (d) 12.5% Cu-Ta_2O_5 thin films.

As the Cu concentration increased, significant variations in the grain size and shape were observed, along with noticeable agglomeration. These changes indicate that Cu plays a role in the growth mechanism by acting as a nucleation center, thus influencing grain formation during film deposition. Pure films exhibited a smoother and denser surface, whereas Cu-doped films showed increased surface roughness and irregularities, which highlight a clear correlation between doping concentration and surface morphology.

EDX analysis was performed to determine the chemical composition and to confirm the incorporation of Cu into the

host matrix of Ta_2O_5. Figure 3 shows the energy-dispersive x-ray spectra of the fabricated thin films of pristine and Cu-incorporated Ta_2O_5. To get the highest counts for the elemental composition analysis, EDX spectra were acquired using a 5 μm spot size and electron beam energy of 15 kV. Ta, Cu, and O peaks were observed in all thin film compositions, indicating the presence of the expected concentrations.

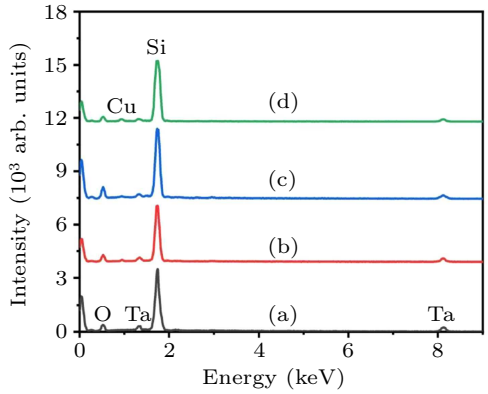


Fig. 3. EDX spectra of (a) pure Ta_2O_5, (b) 4.16% Cu-Ta_2O_5, (c) 6.25% Cu-Ta_2O_5, and (d) 12.5% Cu-Ta_2O_5 thin films.

3.3. Electronic properties

To understand the electronic properties of the material, TDOS and PDOS spectra, indicated by state probability and band structure, were acquired because they were strongly related to the underlying electronic behavior. The band structure illustrates the contribution of valence electrons in the material, whereas the number of states indicates the contribution of intraband and interband transitions as well as substates. Theoretically, TDOS and PDOS investigations can analyze the impact of relaxation on the electronic band structure and atomic exchange.[27] Figures 4(a)–4d) shows the TDOS and PDOS spectra of pure and Cu-doped Ta_2O_5 calculated using DFT+U methods, setting the Fermi level to zero. The density of states computations were performed in the energy range of −6 eV to 6 eV, demonstrating continuous valence and conduction bands.

Figure 4(a) shows the TDOS and PDOS spectra of pure Ta_2O_5, indicating a significant bandgap between the conduction and valence state of 1.5 eV. The main contribution of the valence band is from the O atom, whereas for the conduction band, the Ta atom plays a vital role. According to the PDOS spectra of pure Ta_2O_5, the Ta-d and O-p orbitals mainly contribute to the conduction and valence bands, respectively, leading to p–d hybridization because it refers to the broadening of the electronic states of Ta and O atoms. In the case of pure tantalum oxide, the TDOS calculations exhibited the maxima of the valence band and conduction band at −0.93 eV and 2.36 eV, respectively. It was also observed from the TDOS spectra that as Cu was incorporated in the system, the states of the Ta atom shifted toward the region of the conduction band, resulting in a significant reduction in the bandgap, as shown in Fig. 4(b). It also shows that as Cu was induced in the material, the valence band contribution was mainly attributable to the Ta atom, whereas the Cu atom was responsible for the conduction band contribution, as shown in Figs. 4(c) and 4(d). This variation in the electronic structure was attributable to the increase in the dopant concentration. The results revealed that as the Cu concentration increased, the variation in the electronic states and orbital peaks could be observed along with the valence band shifts toward the conduction band. This reduces the bandgap energy because the electronic states are induced by the positional changes in the valence band. Furthermore, the overlapping states of Cu, Ta, and O cause bonding interactions. Thus, the overlapping of states as an impurity (Cu) is introduced in the host material (Ta_2O_5) increases the number of states and manifests the modified electronic properties. The electronic structure from DFT also showed changes in the density of states (DOS), in which Cu doping introduced new energy levels close to the valence and conduction bands. These changes support the experimental observation of enhanced electrical conductivity because the added states provide additional charge transport paths. The partial density of states (PDOS) further confirmed that Cu d orbitals interact with O p orbitals, which may improve carrier mobility and reduce recombination; these potential properties make this material a potential candidate for optoelectronic applications.

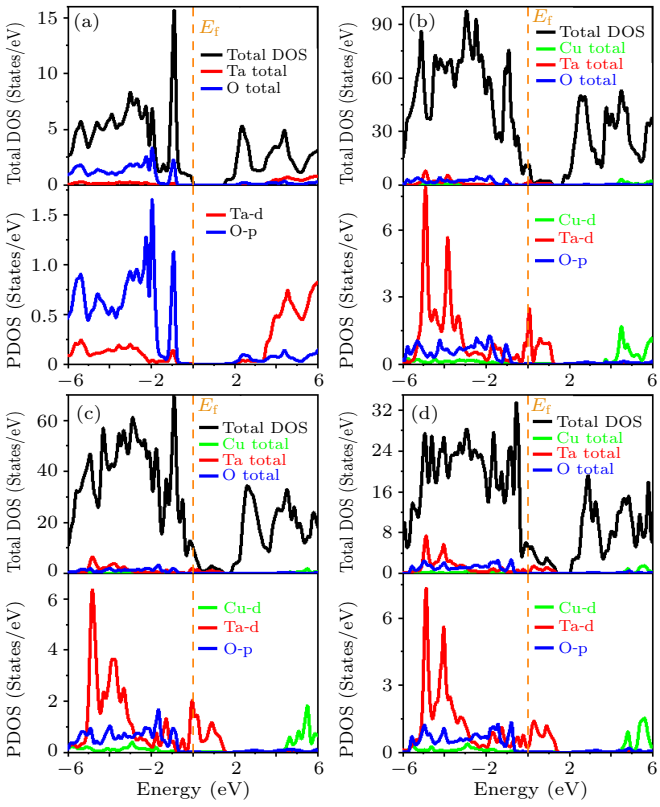


Fig. 4. TDOS and PDOS spectra of (a) pure Ta_2O_5, (b) 4.16% Cu-Ta_2O_5, (c) 6.25% Cu-Ta_2O_5, and (d) 12.5% Cu-Ta_2O_5.

The band structure was examined using the mBJ tech-

nique for exchange–correlation along the higher symmetric boundaries of the Brillouin zone. The graphs illustrate the electronic band structures of pristine and Cu-incorporated Ta_2O_5, as shown in Fig. 5, in which the Fermi energy is located at zero. Figure 5(a) shows that pure Ta_2O_5 has an indirect bandgap of approximately 1.5 eV. The results indicate that the electron mobility increased with the incorporation of Cu, as illustrated in the band structure graphs. The impact of Cu on the band structure can also be observed through the overlapping phenomenon. A shift of the Fermi level toward the valence band was observed, indicating the p-type semiconductor behavior of the doped materials. A noticeable bandgap reduction was observed upon Cu incorporation owing to the generation of energy levels between the conduction and valence bands, which can enable these compositions to be used in optoelectronic devices.

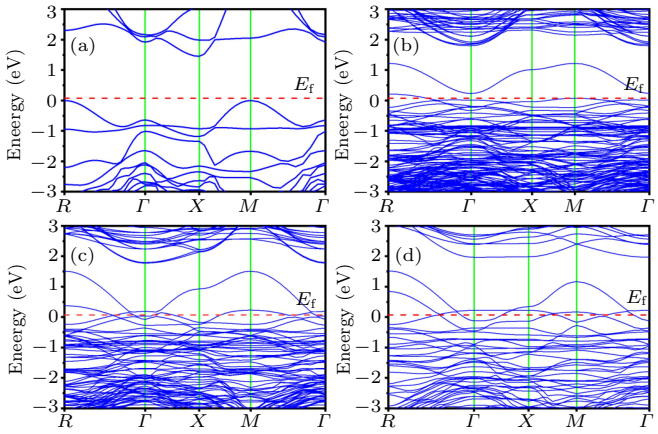


Fig. 5. Band structure plots of (a) pure Ta_2O_5, (b) 4.16% Cu-Ta_2O_5, (c) 6.25% Cu-Ta_2O_5, and (d) 12.5% Cu-Ta_2O_5.

The total and partial densities of states indicate that Cu doping introduced additional electronic states near the Fermi level, effectively reducing the bandgap. This narrowing of the gap enhanced the electrical conductivity by increasing the number of available charge carriers. Furthermore, the shift in the Fermi level and the notable orbital interactions among Cu, Ta, and O atoms indicate stronger chemical bonding and a modified charge distribution, which supports the changes observed in the electrical performance of the material. To support the experimental findings, DFT calculations were performed for Cu-doped Ta_2O_5 at different doping levels. Theoretical results showed that doping with Cu led to a reduction in the bandgap, which was attributed to the introduction of Cu d states near the Fermi level. This trend is in good agreement with the experimentally measured Tauc relation, where a decrease in the optical bandgap was observed with increasing Cu content.

3.4. Thermoelectric properties

The BoltzTraP package, which is integrated into WIEN2k software, was used to analyze the thermoelectric properties (thermal conductivity (κ), electrical conductivity (σ), specific heat capacity, and Seebeck coefficient (S)), as shown in Fig. 6. The structure of an effective thermoelectric material has a large number of free charge carriers, resulting in high electrical conductivity.[28] Figure 6(a) presents the variation in electrical conductivity with temperature for the pure and Cu-doped Ta_2O_5 materials. As the result depicts, the increase in electrical conductivity with an increase in Cu content in the host material might be attributable to the enhancement in charge carriers signifying energy states near the Fermi level, indicating the transport of electrons from VB to CB. The theoretically recorded electrical conductivity values were 1.96 $(\Omega{\cdot}m{\cdot}s)^{-1}$ for pure Ta_2O_5 and 2.61 $(\Omega{\cdot}m{\cdot}s)^{-1}$ at the maximum Cu concentration. Therefore, the findings indicate that an increase in the electrical conductivity would follow an increase in the impurity concentration, which is an indication of the high density of states near the Fermi level. This results in increased mobility with higher Cu content, making it appropriate for thermoelectric materials.

Thermal conductivity, which is associated with electron and phonon interaction, is a crucial component in examining the capacity of thermal insulation because it provides insights into the transport of heat within a material.[29] Figure 6(b) shows the graph of κ of pristine and Cu-incorporated Ta_2O_5 with temperature variation. It can be observed that κ increased with increasing temperature because the temperature increment improved the carrier mobility. The observed thermal conductivity values were 1.29 $W{\cdot}m^{-1}{\cdot}K^{-1}$ for pure Ta_2O_5 and 5.74 $W{\cdot}m^{-1}{\cdot}K^{-1}$ at the maximum Cu concentration. The results revealed an enhancement in thermal conductivity as Cu was introduced in the material, depicting the diffusion of Cu into the lattice.

Figure 6(c) presents the graph of the thermoelectric power S with the temperature variation of the pure and Cu-doped Ta_2O_5 materials. It revealed a decrease in the Seebeck coefficient with increasing Cu concentration. All samples have a positive Seebeck coefficient, and S appears to be zero at $T = 0$ K. These results indicate that the samples are p-type materials, in which hole carriers are dominant. The calculated Seebeck coefficient values were 3.66 $\mu V{\cdot}K^{-1}$ for pure Ta_2O_5 and 1.91 $\mu V{\cdot}K^{-1}$ at the maximum Cu concentration. Figure 6(d) shows the variation in specific heat with respect to T. As the Cu concentration increased, the specific heat of the material increased, which might have been caused by the vibration and translation effects. The recorded specific heat values were 0.73 J/K·kg for pure Ta_2O_5 and 11.6 J/K·kg at the maximum Cu concentration.

Thermoelectric analysis indicates that with increasing Cu concentration, the electrical conductivity improved, whereas the Seebeck coefficient declined, an expected behavior associated with a higher carrier concentration. The observed increase in thermal conductivity with Cu doping indicates that

the introduced Cu atoms not only boost the carrier mobility but also enhance heat transport. These observations follow the fundamental thermoelectric theory, in which doping influences the relationship between electrical and thermal properties.

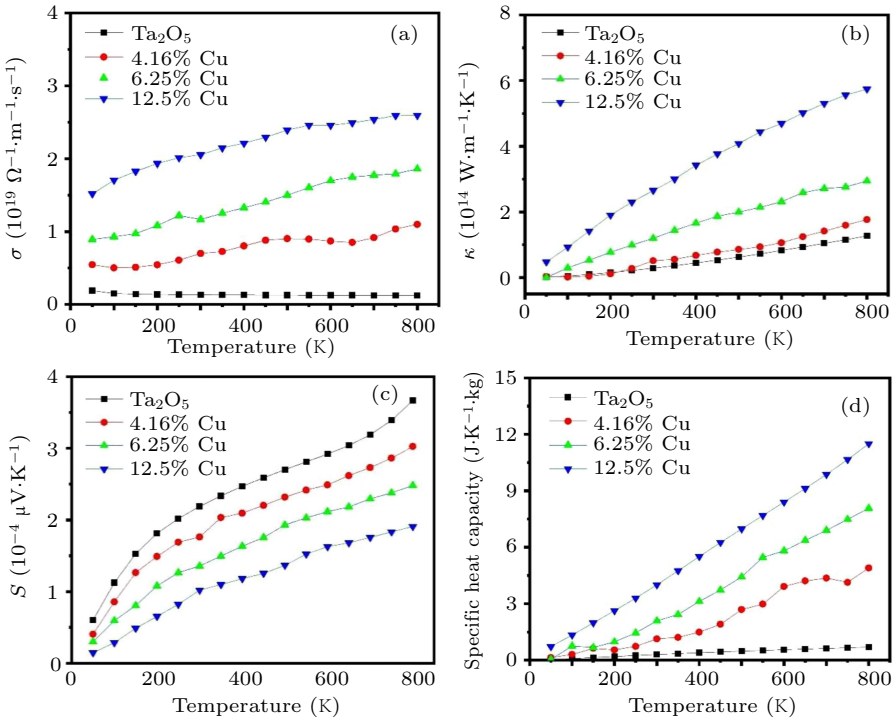


Fig. 6. Thermoelectric properties of (a) pure Ta_2O_5, (b) 4.16% Cu-Ta_2O_5, (c) 6.25% Cu-Ta_2O_5, and (d) 12.5% Cu-Ta_2O_5.

3.5. Optical properties

Figures 7 and 8 show the optical properties that are energy dependent, such as optical conductivity, extinction coefficient, real epsilon, refractive index, absorption coefficient, reflectivity (R), and bandgap of undoped and Cu-doped Ta_2O_5. These properties were evaluated experimentally using spectroscopic ellipsometry and theoretically using DFT with the WIEN2K software.

The absorption coefficient measures the ability of a material to absorb light at different wavelengths. It can be computed mathematically using the real and imaginary dielectric constants as[30]

$$\alpha(\omega) = \sqrt{2}\left[\sqrt{\varepsilon_1^2(\omega)+\varepsilon_2^2(\omega)} - \varepsilon_r(\omega)\right]^{1/2}.$$

Figure 7(a) illustrates α of the simulated data concerning energy variation, which increased with the introduction of Cu in the system. Additionally, the experimentally recorded absorption coefficient graphs show that the value increases with energy, peaking in the high-energy region. Figure 8(a) presents the experimental data, showing that the absorption coefficient increases with increasing Cu concentration. All materials showed 0% absorption on the composite surface when no incident photons were present. The simulation data revealed that with the addition of Cu, absorption edges can be observed near the IR to the visible region because of the enhancement in DOS near the band edge. The experimental data show that the absorption edge of 12.5% Cu-Ta_2O_5 occurred at 2.7 eV, indicating a blue shift in the absorption spectrum and suggesting its potential for high-frequency applications. This blue shift may be attributed to quantum confinement effects, which can improve the electrical properties of Ta_2O_5 materials. The minor peaks appearing at lower energy values can be attributed to the formation of electronic states, as shown in the DOS plots (Fig. 4). Moreover, the differences between the theoretical and experimental absorption calculations could be attributed to differences in methodology.

Optical conductivity can be calculated from the α and n relation given as[30]

$$\alpha\pi\sigma = \frac{nc}{4}.$$

Optical conductivity defines the suitability of a material for optoelectronic devices. Figures 7(b) and 8(b) show the optical conductivity plots versus energy for the theoretical and experimental data. It increases in both cases as the photon energy increases. The experimental results show an increase in σ with increasing Cu concentration. Simulated curves show the conducting humps at energies 0.15 eV, 0.76 eV, and 1.31 eV until maximum conductivity is obtained in Cu-doped Ta_2O_5 materials. A significant increase in conductivity can be observed at higher energy levels or in the UV region, which might be due to the carrier mobility and interband transitions, whereas the absorption of electromagnetic radiation is related to an increase in the conductivity of the material. A similar pattern was observed in the experimental data, indicating a correlation between the simulated and experimental results.

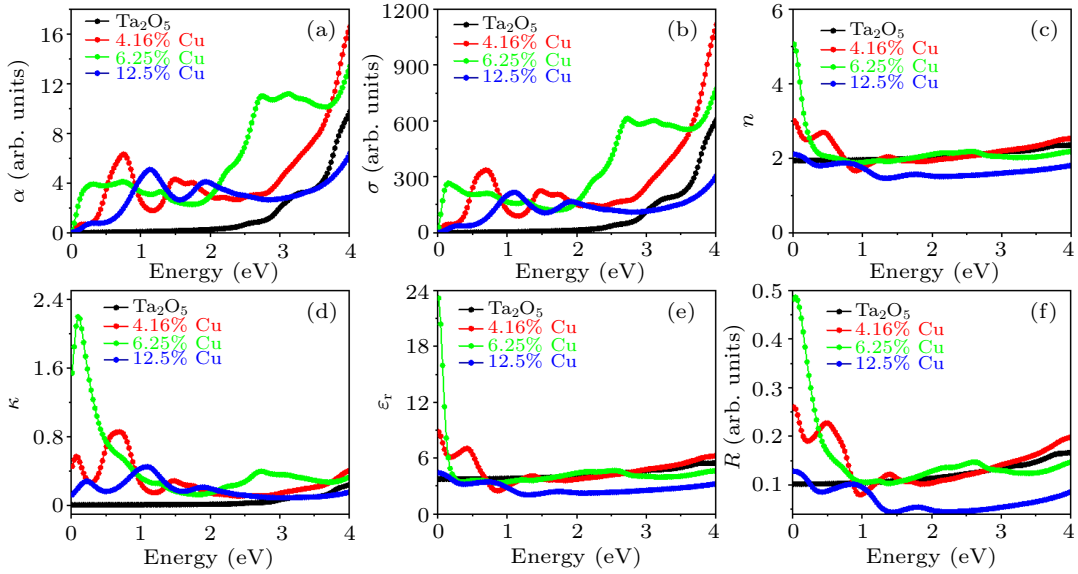


Fig. 7. Optical parameters calculated through DFT: (a) absorption coefficient α, (b) optical conductivity σ, (c) refractive index n, (d) extinction coefficient K, (e) real epsilon ε_r, and (f) reflectivity R of pure and Cu doped Ta_2O_5.

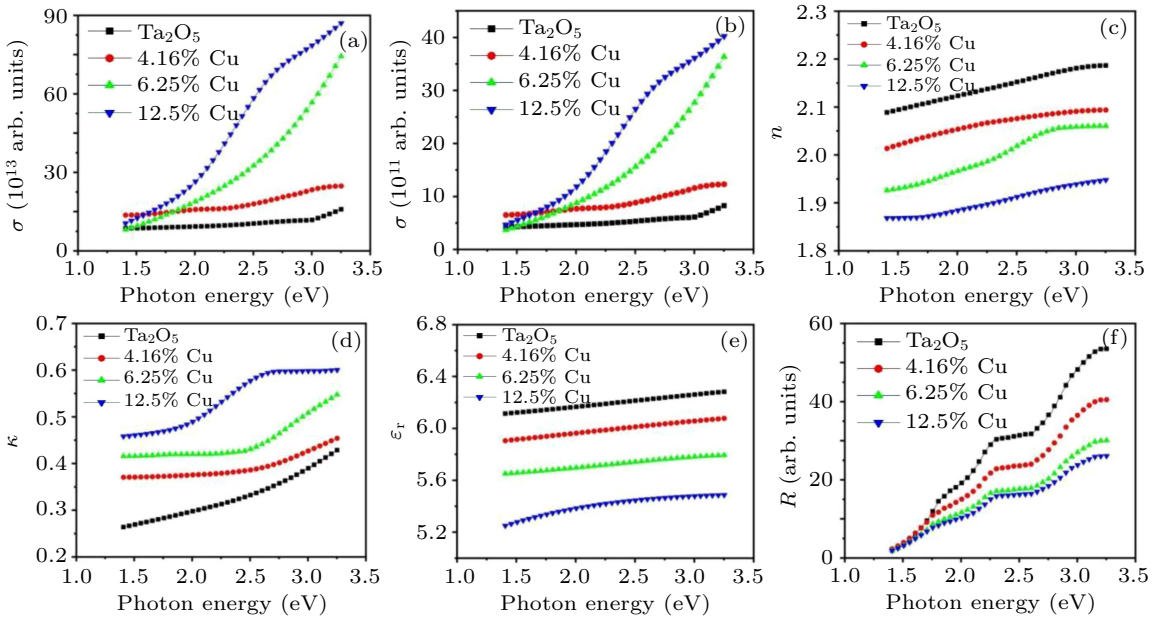


Fig. 8. Optical parameters calculated through ellipsometry: (a) absorption coefficient α, (b) optical conductivity σ, (c) refractive index n, (d) extinction coefficient K, (e) real epsilon ε_r, and (f) reflectivity R of pure and Cu doped Ta_2O_5.

The refractive index is a dimensionless number that indicates how much light bends or refracts when entering a medium from a vacuum or another medium, such as[30]

$$n(\omega) = \left[\frac{\varepsilon_1(\omega)}{2} + \frac{\sqrt{\varepsilon_1^2(\omega)+\varepsilon_2^2(\omega)}}{2}\right]^{1/2}.$$

The refractive indices of pure and Cu-based Ta_2O_5 compositions were calculated using theoretical and experimental methodologies, as illustrated in Figs. 7(c) and 8(c). The simulated curves exhibit the maximum refractive index values in the initial region and then decline with an increase in energy, whereas the static refractive index of a material determines the velocity of the electromagnetic wave. The simulated data show a static refractive index of 1.93 for pure Ta_2O_5, whereas Cu-doped samples with concentrations of 4.16%, 6.25%, and 12.5% exhibit values of 3.05, 5.07, and 2.11, respectively. The experimental curves revealed that the refractive index increased with photon energy but decreased with increasing Cu content in the host material, showing similar behavior for all compositions.

The extinction coefficient measures the amount of light lost due to absorption and scattering per unit distance in a medium. Mathematically, it can be derived from the relation[30]

$$k = \frac{\lambda\alpha}{4\pi}.$$

Figures 7(d) and 8(d) show the simulated and experimental curves of the extinction coefficient with respect to photon en-

ergy. In the simulated curves, a sudden increase was observed in the lower energy region, followed by a decline as energy increased, whereas the experimental curves show that as the concentration of Cu increased in the material, its extinction coefficient also increased. According to Mae's theory, the improvement in the full-width half-maxima of excitonic peaks explains the excitonic peak of the material, which is dependent on the grain or particle size. The extinction curves suggest the feasibility of these materials for photovoltaic applications because they reach their highest values in a higher energy range, as shown in Fig. 8(d).

The simulated and experimental curves of the real epsilon are shown in Figs. 7(e) and 8(e). Using Kramer–Koring transformations, they can be calculated using[30]

$$\varepsilon_{\mathrm{r}} = 1 + \frac{2}{\pi}\rho_0 \int_0^{\infty} \frac{\omega' \varepsilon_{\mathrm{i}}(\omega)}{\omega'^2 - \omega^2}\,\mathrm{d}\omega.$$

The real part of the dielectric constant represents a material's ability to store energy from an electric field, which influences how light propagates through the material. A static dielectric is referred to as the value of ε_{r} at zero energy. The recorded values were 8.91, 23.34, and 4.57 for the 4.16%, 6.25%, and 12.5% Cu-doped Ta_2O_5 compositions, respectively, whereas that of pure Ta_2O_5 was 3.75. As Cu was added into the system, its static dielectric constant increased, which might be related to the bandgap reduction; therefore, electronic transitions need less energy to enhance the value of the static dielectric constant. The experimental curves exhibit a decrease as Cu was introduced into the system, which might be associated with the fact that an electromagnetic field does not change the dipole orientation.

Reflectivity is the proportion of incident light reflected off a surface, indicating how much light is not absorbed or transmitted by a material. Theoretically, the following relation can be used to calculate this:[30]

$$R(\omega) = \left[\frac{\sqrt{\varepsilon_1(\omega) + \mathrm{i}\varepsilon_2(\omega)} - 1}{\sqrt{\varepsilon_1(\omega) + \mathrm{i}\varepsilon_2(\omega)} + 1}\right]^2.$$

For pure and Cu-doped Ta_2O_5, the variations in reflectivity curves with respect to energy are shown in Figs. 7(f) and 8(f) for the simulated and experimental data, respectively. The reflectivity curves of the simulated data exhibited a sudden increase at 0 eV energy and decreased exponentially with increasing photon energy. The experimental results showed an increase in reflectivity with increasing energy, and the maximum value was observed in the energy range of 3.1–3.4 eV. Cu incorporation decreased the reflectivity, contradicting the simulated data. These possible differences can be attributed to the difference between the theoretical and experimental parameters.

The optical properties of Cu-doped Ta_2O_5 were studied using both DFT calculations and spectroscopic ellipsometry, and almost consistent results were obtained. The DFT analysis showed a reduction in the bandgap and an increase in the optical absorption owing to the presence of Cu d states near the Fermi level. These states enhance the interaction of the material with the incident light, as indicated by the ellipsometry data, which showed increased values of the extinction coefficient with Cu doping. The close agreement between the calculated dielectric function and experimental optical data confirms the accuracy of the theoretical method and shows that Cu doping has a significant impact on the optical behavior of Ta_2O_5.

The absorption edge can be used to experimentally determine the optical bandgap value. When there is uncertainty in the excitonic peaks, it becomes difficult to determine the band energy. In these situations, the Tauc relations aid in estimating the bandgap energy. The following relation can be used to determine the bandgap:[31]

$$(\alpha h\nu)^{1/n} = A(h\nu - E_{\mathrm{g}}),$$

where α is the absorption coefficient, h is Planck's constant, ν is the photon frequency, A is the proportionality constant, and n is the indirect or direct transition with value of 1/2 or 2, respectively. The bandgap values and other optical parameters of Ta_2O_5 are listed in Table 2. Figure 9 presents a Tauc plot for the bandgap, where it can be observed that the bandgap decreased as the Cu concentration increased in Ta_2O_5, making it a potential material for optoelectronic applications.

Table 2. Optical parameters of pure Ta_2O_5 compared with those reported in the literature.

Optical parameters	This study	Previous studies
Refractive index	1.93	1.92[32]
Real epsilon	3.75	5.92[33]
Extinction coefficient	0.25	0.12[34]
Bandgap (eV)	2.61	3.8[35]

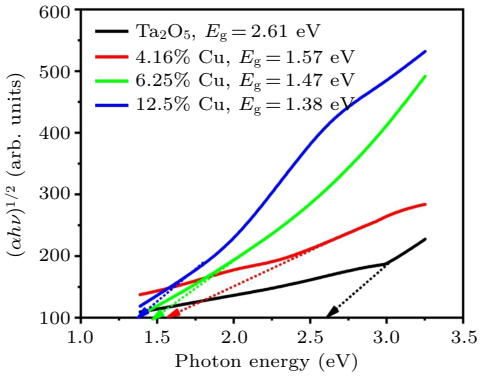


Fig. 9. Tauc plot of pure and Cu-doped Ta_2O_5 thin films.

This study combines DFT calculations with experimental results to clearly show how Cu doping affects the properties of Ta_2O_5. The results demonstrate that DFT is a useful tool for predicting material behavior and helping to design better experiments. This combined approach improves the understanding of how defects change materials and supports the development of doped metal oxides for advanced uses. The

optical properties clearly demonstrated the effect of Cu doping on the structure of the material. The absorption coefficient increased as new energy states formed near the band edge owing to the inclusion of Cu. A significant blue shift in the absorption edge indicated the presence of quantum confinement effects. Furthermore, variations in the refractive index, extinction coefficient, and dielectric constant with doping confirmed the changes in the electronic structure. The consistency between the experimental results and theoretical findings further validated the modifications in the optical properties caused by Cu doping.

4. Conclusion

This study aimed to investigate the structural, electronic, thermoelectric, and optical properties of Cu-doped Ta_2O_5 thin films using both theoretical and experimental approaches. DFT calculations predicted the response of the material under the modified Becke–Johnson approximation, whereas DC magnetron sputtering was used to synthesize phase-pure thin films. The PDOS spectra indicate that the Ta-d and O-p orbitals dominated the conduction and valence bands, leading to p-d hybridization. The TDOS spectra revealed that Cu doping caused a shift in the Ta states toward the conduction band, significantly reducing the bandgap. The thermoelectric parameters varied considerably. The XRD analysis confirmed an orthorhombic structure with (110) and (019) orientations. In terms of the optical properties, the absorption coefficient increased, making Cu-doped Ta_2O_5 suitable for photovoltaic applications. These findings demonstrate that the incorporation of Cu effectively modified the structural and electronic properties, enhancing the potential of Ta_2O_5 for thermoelectric and optoelectronic applications.

Acknowledgements

The authors extend their appreciation to the Deanship of Research and Graduate Studies at King Khalid University, Saudi Arabia, for funding this study through the Large Groups Project (Grant No. RGP2/2/47). The authors extend their appreciation to the Deanship of Scientific Research at Northern Border University, Arar, KSA for funding this research work through project number NBU-FFR-2025-1902-02.

References

[1] Kar K K 2020 *Handbook of Nanocomposite Supercapacitor Materials II: Performance* (Cham: Springer International Publishing AG)
[2] Danish Mohd, Pandey A, Ansari Mohd O and Jilani A 2017 *J. Mater. Sci.: Mater. Electron.* **28** 6812
[3] Naveenraj S, Lee G J, Anandan S and Wu J J 2015 *Mater. Res. Bull.* **67** 20
[4] Li Q, Liang C, Tian Z, Zhang J, Zhang H and Cai W 2012 *CrystEngComm* **14** 3236
[5] Delaportas D, Svarnas P and Alexandrou I 2010 *J. Electrochem. Soc.* **157** K138
[6] Dezelah, Wiedmann M K, Mizohata K, Baird R J, Niinistö L and Winter C H 2007 *J. Am. Chem. Soc.* **129** 12370
[7] Agrawal M, Pich A, Gupta S, Zafeiropoulos N E, Simon P and Stamm M 2008 *Langmuir* **24** 1013
[8] Devan R S, Ho W D, Chen C H, Shiu H W, Ho C H, Cheng C L, Wu S Y, Liou Y and Ma Y R 2009 *Nanotechnology* **20** 445708
[9] Devan R S, Gao S Y, Ho W D, Lin J H, Ma Y R, Patil P S and Liou Y 2011 *Appl. Phys. Lett.* **98** 133117
[10] Devan R S, Lin C L, Gao S Y, Cheng C L, Liou Y and Ma Y R 2011 *Phys. Chem. Chem. Phys.* **13** 13441
[11] Sathasivam S, Williamson B A D, Kafizas A, Althabaiti S A, Obaid A Y, Basahel S N, Scanlon D O, Carmalt C J and Parkin I P 2017 *J. Phys. Chem. C* **121** 202
[12] Miura K, Osawa T, Yokota Y, Suzuki T and Hanaizumi O 2014 *Results Phys.* **4** 148
[13] Khalil M, Qureshi M T, Elaimi M A, Aamir L, Ahmad M, Saleem M and Saleem M 2024 *Results Phys.* **67** 108041
[14] Le Y, Ma X, Xiao H, Luan C, Zhang B and Ma J 2023 *Appl. Phys. Lett.* **122** 252103
[15] Suzuki T M, Saeki S, Sekizawa K, Kitazumi K, Takahashi N and Morikawa T 2017 *Appl. Catal. B: Environmental* **202** 597
[16] Krishnan R R, Vinodkumar R, Rajan G, Gopchandran K G and Mahadevan Pillai V P 2010 *Mater. Sci. Eng. B* **174** 150
[17] Araña J, Doña-Rodríguez J M, Melián J A H, Rendón E T and Díaz O G 2005 *J. Photochem. Photobiol. A: Chemistry* **174** 7
[18] Manivel A, Naveenraj S, Sathish Kumar P S and Anandan S 2010 *Sci. Adv. Mater.* **2** 51
[19] Liu C, Liu Z, Li J, Li Y, Han J, Wang Y, Liu Z and Ya J 2013 *Microelectron. Eng.* **103** 12
[20] Martin P J, Bendavid A, Swain M, Netterfield R P, Kinder T J, Sainty W G, Drage D and Wielunski L 1994 *Thin Solid Films* **239** 181
[21] Lee J S, Chang S J, Chen J F, Sun S C, Liu C H and Liaw U H 2003 *Mater. Chem. Phys.* **77** 24
[22] Miura K, Osawa T, Yokota Y, Hossain Z and Hanaizumi O 2015 *MSCE* **03** 47
[23] Khalil M, Bashir A, Ullah F, Ramay S M and Saleem M 2024 *J. Electron. Mater.* **53** 1823
[24] Khalil M, Bashir A, Khalil U, Ullah F, Ramay S M and Saleem M 2024 *ECS J. Solid State Sci. Technol.* **13** 084003
[25] Geretovszky Z, Szörényi T, Stoquert J P and Boyd I W 2004 *Thin Solid Films* textbf453–454 245
[26] Al-Kuhaili M F 2021 *Mater. Chem. Phys.* **257** 123749
[27] Thapa R, Bhattarai B, Kozicki M N, Subedi K N and Drabold D A 2020 *Phys. Rev. Mater.* **4** 064603
[28] Hedhili F, Khan H, Sohail M, Rahman N, Khan R, Alahmad W, Albaqawi H S, Al-Shomar S M and Alsalmi O 2023 *Molecules* **28** 4418
[29] Riaz S, Yaseen M, Butt M K, Mubashir S, Iqbal J, Altowyan A S, Dahshan A, Murtaza A, Iqbal M and Laref A 2021 *Mater. Sci. Semicond. Process.* **133** 105976
[30] Soussi A, Ait Hssi A, Boujnah M, Boulkadat L, Abouabassi K, Asbayou A, Elfanaoui A, Markazi R, Ihlal A and Bouabid K 2021 *J. Elec. Mater.* **50** 4497
[31] Khalil M, Bashir A, Ullah F, Ramay S M and Saleem M 2025 *Mater. Sci. Eng.: B* **319** 118374
[32] Ghodsi F E, Tepehan F Z and Tepehan G G 1997 *Thin Solid Films* **295** 11
[33] Valencia B C, Pérez W S and Osorio G J M 2018 *TecnoLógicas.* **21** 43
[34] Thapliyal P, Panwar N S and Rao G M 2021 *Superlattices Microstruct.* **158** 107008
[35] Gurylev V 2022 *Mater. Today Sustainability* **18** 100131